

Wadi El-Gemal Tourmaline-Bearing Deposits, Southern Eastern Desert, Egypt: Constraints on Petrology and Geochemistry

Mohamoud M. El-Rahmany¹, Gehad M. Saleh², Hatem M. El-Desoky¹, Hamada M. El-Awny¹

1. Department of Geology, Faculty of Science, Al-Azhar University, Cairo, Egypt

2. Nuclear Materials Authority (NMA), Cairo, Egypt

ABSTRACT: This paper seeks to characterize the petrology and geochemistry of Wadi El-Gemal tourmaline deposits, South Eastern Desert, Egypt. Wadi El-Gemal district includes Um El-Debbaa, Wadi Nugrus (Um Slimite), Wadi Sikait and Wadi Abu Rusheid regions. Tourmaline-bearing schists occur chiefly in Neoproterozoic basins dominated by arc volcanoclastic metasediments rocks. Principal hosts are metapelites and metapsammites, with locally abundant metapsammopelites (greenschist and amphibolite facies). Within Wadi El-Gemal regionally metamorphosed terranes tourmaline-bearing schists display moderate to strongly foliated fabrics. Grain sizes range from < 5 mm in dense foliated varieties to > 1cm in more foliated samples. The petrographic features of the tourmaline occurrences vary, and allow its classification into seven groups, depending on the host rock lithology, mineral assemblage and their relative abundance. Their relative abundance varies considerably from one locality to another. The modal composition of the studied tourmaline-bearing schists reveals that they have a wide range of mineral assemblages. The petrochemical characteristics of the tourmaline-bearing schists are of peraluminous in nature and the source rocks originated from calc-alkaline magma. They seem to have been evolved in an island arc tectonic setting, where they are related to immature island arcs. These schists are high pressure and low temperature, amphibolite facies and kyanite zone due to regional and metasomatic metamorphism.

1. Introduction

The present paper deals with geology, petrography and geochemistry of Wadi El-Gemal tourmaline-bearing deposits, South Eastern Desert, Egypt. Wadi El-Gemal district include four areas of Um El-Debbaa, Um Slimite, Wadi Sikait and Wadi Abu Rusheid (Fig.1). The study district is located at the northern part of the Southeastern Desert. It is easily accessible through the Red Sea Highway to the eastern entrance of Wadi El-Gemal desert track at about 52 km, south of Mersa Alam coastal city. The highest peak is Gabal Sikait formed of serpentinites and related rocks surrounded by rounded hillocks and mounds of ophiolitic mélange.

The study area consists of medium to low relief hills with many high to moderate mountain peaks. The most important peaks are: Gabal Um Kabu (639 m), Gabal Nasb El-Madara (452 m), Gabal Um Harba and Gabal Sikait (769m), which form contrasted relief with the surrounded low lands occupied by ophiolitic mélange. The highest peak is Gabal Sikait formed of serpentinites and related rocks surrounded by rounded hillocks and mounds of ophiolitic mélange.

Wadi El-Gemal Basin is considered one of the prominent geomorphological features in the Eastern Desert of Egypt. Few geomorphological studies were carried out on Wadi El-Gemal (Hegazy, 1984; Akawy, 1999; Ahmed, 2001; Khaleal, 2005 and Mahmoud, 2005). Wadi El-Gemal basin is a seventh order basin; its drainage net is well developed, dense and has variable

angles of juncture. The large channels are mostly arranged in parallel to subparallel patterns with dendritic to sub-dendritic tributaries. Trellis to sub-trellis drainage patterns is locally developed. The main Wadi is oriented NW-SE in upper part, E-W in middle part and NE-SW at the mouth (Akawy, 1999).

2. Materials and Methods

Field work included sampling and descriptions of the exposed rock units (32 samples). Petrographical studies of a total of 24 thin sections using the polarizing microscope. The chemical analyses of major oxides, trace and rare earth elements of the studied tourmaline-bearing schists were carried out at the Central laboratories of the Nuclear Materials Authority (NMA), Egypt. The geochemical characterization of the Wadi El-Gemal tourmaline-bearing schists encountered in the studied areas are carried out through the study of the chemical composition of 24 selected samples collected from Um El-Debbaa, Wadi Nugrus (Um Slimite), Wadi Sikait and Wadi Abu Rusheid. 12 samples were selected for the determination of the rare earth elements and the results of the chemical analyses are given in Tables (1, 2 and 3).)

3. Geologic Setting and Petrography Tourmaline deposits

The exposed rock units at the studied district are ophiolitic rocks (Ultramafic rocks and layered metagabbros), arc volcanoclastic metasediments, cataclastic rocks, granitic rocks (Alkali feldspar granite, muscovite granite, porphyritic biotite granite) and post granitic dykes and veins (Fig.2).

Tourmaline-bearing schists are found in arc volcanoclastic metasediments (mélange rocks), are the dominant rock variety in the areas and the main target of the present study, forming a large exposure of low to moderate relief extending between the muscovite granites and mélange rocks (Fig.3a, b, c & d). The mélange schists were proposed by El-Desoky (2010) at the studied regions. These rocks are classified according to their low to medium grade of metamorphism (greenschist facies up to amphibolite facies) into the following: Talc schists, tremolite-graphite schists, tremolite-actinolite schists, mica schists, biotite schists and biotite-garnetiferous schists (El-Desoky, 2010). The striking feature of these schists is the microscopic variation of grain size, grain shape and grain boundaries. This textural heterogeneity is a typical feature of dynamic metamorphism (Mason, 1978).

The petrographic features of the tourmaline occurrences vary, and allow its classification into seven groups, depending on the host rock lithology, mineral assemblage and their relative abundance.

Graphite - tremolite - tourmaline schists found in Um El-Debbaa area and consisted of tourmaline (60.47%), tremolite (21.62%) and graphite (16.18%) in decreasing order of abundance. Opaque mineral (1.15%) is a widely scattered accessory constituent, whereas rutile (0.58%) is a minor accessory. They are medium- to coarse-grained displaying schistose texture and brownish color. The tourmaline is very strongly characterized under the microscope. It shows strong negative birefractance; also a rather high index of refraction and very striking pleochroism. Tourmaline occurs as medium- to coarse-grained, idiomorphic prismatic crystals and exhibit two sets of cleavage, hexagonal crystals (Fig.4a & b). They display complex twinning and irregular zoning, brownish color, from 2 - 13 mm in length and 2 - 3mm in width. It is fairly pleochroic in shades of pale brown. Most tourmaline grains are optically unzoned, but

in a few thin sections some tourmalines have dark brown interiors and paler rims. It frequently contains tremolite, graphite, rutile and opaque minerals inclusions (Fig.4c & d).

Graphite-tourmaline-tremolite schists are quite similar to the graphite – tremolite – tourmaline schists, but contain different relative abundance of mineral assemblages. These schists are found in Um Simate area and consist essentially of graphite (23.2%), tourmaline (34.82%) and tremolite (38.52%) with accessory of rutile (1.76%) and opaque minerals (1.7%). Well-developed crystals of tourmaline intercalated with crystals of rutile and opaque minerals (Fig.5a, b, c & d).

Graphite-tourmaline schists are found in Wadi Abu Rusheid area and they possess a hypidiomorphic granular texture and are composed chiefly of tourmaline (68.93%) and graphite (24.99%). The proportions of both minerals can vary appreciably. If the tourmaline content is low the rock resembles tourmaline-graphite schists. Even in that case the term tourmaline-graphite schists will be used for convenience. Rutile (0.5%), tremolite (3.83%) and opaque minerals (1.75) are common accessories. These schists are foliated, porphyroblastic and schistose textures. Tourmaline occurs as brownish inequidimensional hexagonal porphyroblasts wrapped with a matrix of fine-grained graphite and tremolite, stretched parallel to the schistosity. It shows pleochroic from pale yellow to yellowish brown, medium- to coarse-grained, from 1 - 2cm in length and from 2 –3mm in width (Fig.6a & b). It frequently contains tremolite, graphite, rutile and opaque minerals inclusions and exhibit poikiloblastic texture. This due to tourmaline was formed after tremolite, graphite, rutile and opaque minerals (Fig.6a, b, c & d).

Tourmaline-graphite schists are similar to the previously described graphite – tourmaline schists, but are richer in graphite and contain less amount of tourmaline. They are chiefly composed of graphite (61.4%) and tourmaline (35.77%) together with accessory tremolite (0.92%), rutile (1.01%) and opaque minerals (0.91%). The tourmaline – graphite schists are medium- to coarse-grained, displaying schistose texture and brownish color and exposed at Wadi Sikait area. Tourmaline grains are typically zoned with pale yellowish-brown cores (Fig.7a). Frequently with numerous inclusions of graphite, tremolite, rutile and opaques (Fig.7b, c & d) and the rims are dark yellow-brown in tremolite poor rocks.

Tourmaline (65.23%) and quartz (26.98%) are the essential components of **tourmalinites**. The accessory minerals are rutile (1.72%), graphite (3.54%), actinolite (1.03%) and opaque minerals (1.5%). It is a medium- to coarse-grained rock consisting mainly of large equigranular anhedral quartz grains and tourmaline prisms surrounded by numerous slender radiating aggregates of tourmaline. These rocks are found in Um El Debbaa, Wadi Nugrus (Um Simate) and Wadi Sikait areas. Immature crystals of tourmaline disseminated within quartz crystals, they displaying schistose texture (Fig.8a & b). Tourmaline porphyroblastics contains minor crystals of tremolite, graphite, rutile and opaque minerals (Fig.8c & d).

The plagioclase-tourmaline schist is medium- to coarse-grained, and the tourmaline shows poorly-developed foliation and found in Wadi Abu Rusheid area. They are phaneritic, holocrystalline and weakly porphyritic to equigranular. The main constituents are tourmaline (68.45%) and plagioclase (29.41%). Biotite is rare compared to other constituents. Accessory minerals are rutile (1.12%) and opaque minerals (1.02%). Tourmaline is present within the deformed host-rocks. Tourmaline shows a brecciated texture, inductile the brittle deformation and formation under subsolidus conditions. Tourmaline is subhedral to euhedral

with variable grain size (50_800 μ m). It is brown to brownish yellow in color and shows rare optical zoning (Fig.9a, b & c), with inclusions of rutile and opaque minerals (Fig.9c).

Axinite-tremolite-actinolite schists are composed essentially of tremolite-actinolite (81.6%) and opaque minerals (9.7%). The accessory minerals are represented by subordinate amounts of axinite (8.7%). They are fine- to very fine-grained, green to greenish gray in color, well foliated and of schistose texture and present in Wadi Sikait and Wadi Abu Rusheid areas. The alterations demonstrate that these schists are subjected to medium temperature and pressure. These schists are fine- to medium-grained with schistose texture and rich in tremolite-actinolite and late axinite (Fig.10a, b, c & d). This axinite was interpreted as a result of metasomatism with introduction of boron and silicon into the tremolite-actinolite schists in connection with intrusions of granites or granodiorite. The late axinite is invariably enclosed by the abundant of tremolite-actinolite and opaque minerals.

4. Tourmaline Deposits Geochemistry

The analyzed tourmaline-bearing schist samples correspond to the most tourmaline-rich rocks distinguished on the basis of their high B contents. Whole - rock data for the studied tourmaline-bearing schists show limited variations in major and minor element concentrations. These variations mainly reflect the relative proportion of tourmaline versus relic fragments of host schists. Tourmaline is however the main mineral component, exceeding 70% volume of total rock. Through comparison of the studied tourmaline-bearing schists, it can be shown that the tourmaline-bearing schists are richer in MgO, Cr, Ni, Zn, Rb, Y, Ga, V, Nb and B, and poorer in Fe₂O₃, Ba, Th and U, relative to world tourmaline-rich rocks (Table 4). The studied tourmaline-bearing schists have narrow range of SiO₂, Al₂O₃, MgO, CaO, FeO and Fe₂O₃ related to the petrographical of the recorded seven rock types. Also they are poor in Na₂O, K₂O and TiO₂ oxide contents. The trace and REE elements data are presented in Tables (2 and 3).

The contents of **B** are extraordinary high in all samples, range from (2140 - 240 ppm) because of the presence of tourmaline. The contents of Cr, Ni, Zr, V, Sr and Nb are extraordinary high in all samples, Zn contents are comparatively high (4326- 692 ppm), Pb (1465-417ppm) and Ga (489-123ppm) in Wadi Abu Rusheid area. Rb contents are high (702-433 ppm) in Um Slimat area, U and Th contents comparatively low (5 ppm U and 17 ppm Th). The distributions of other trace elements don't show proper variation.

4.1. Chemical composition of the protoliths

The geochemical classification of protoliths for the studied tourmaline-bearing schists was chemically confirmed by plotting the analyses on the ACF, A'KF, SiO₂ - (CaO+Na₂O+K₂O) - (FeO*+MgO+MnO), and (Al₂O₃) - (CaO+Na₂O) - (K₂O) diagrams.

The ACF diagram (Fig.11a) suggested by **Fyfe et al. (1958)** shows that the analyzed tourmaline-bearing schists fall in the fields of pelitic and magnesian hornblende protoliths. On the A'KF diagram (Fig.11b) proposed by **Winkler (1976)**, the analyzed samples fall in and nearby the field of metapelites protoliths.

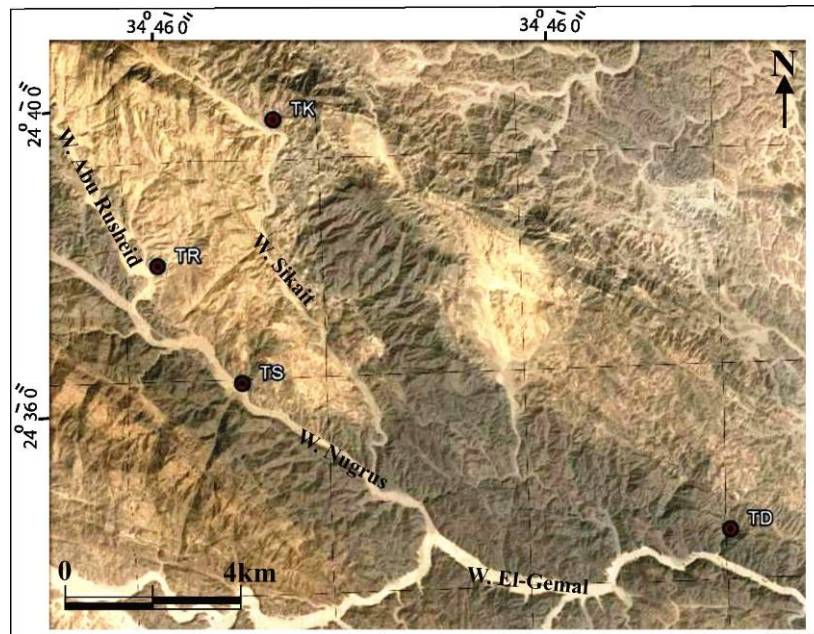


Fig.1. Location map showing Wadi El-Gemal tourmaline deposits samples, SED, Egypt. TR= Wadi Abu Rusheid, TS= Um Slimate, TK= Wadi Sikait and TD= Um El-Debbaa.

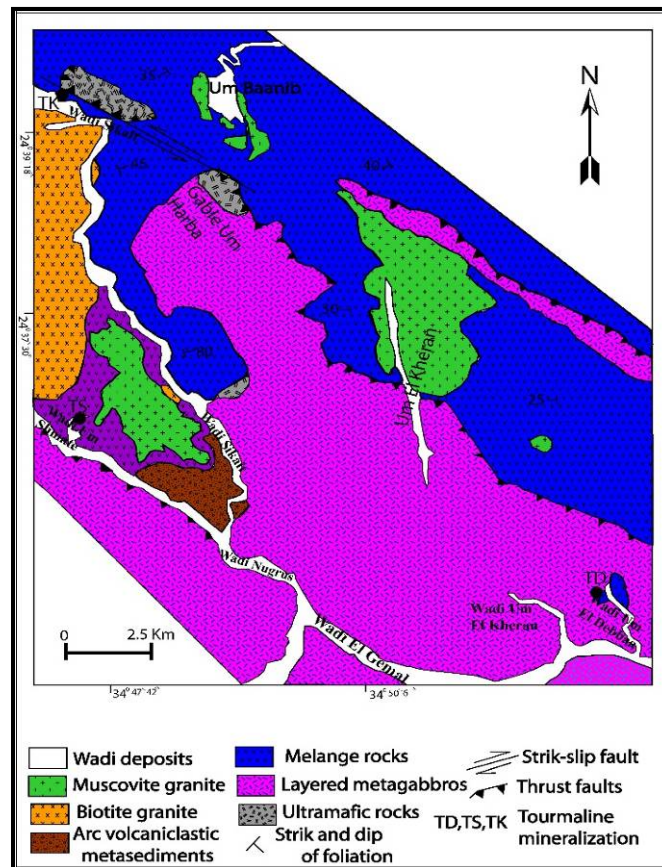


Fig.2. Regional geologic map of the studied regions (modified after [Saleh, 2014](#)).

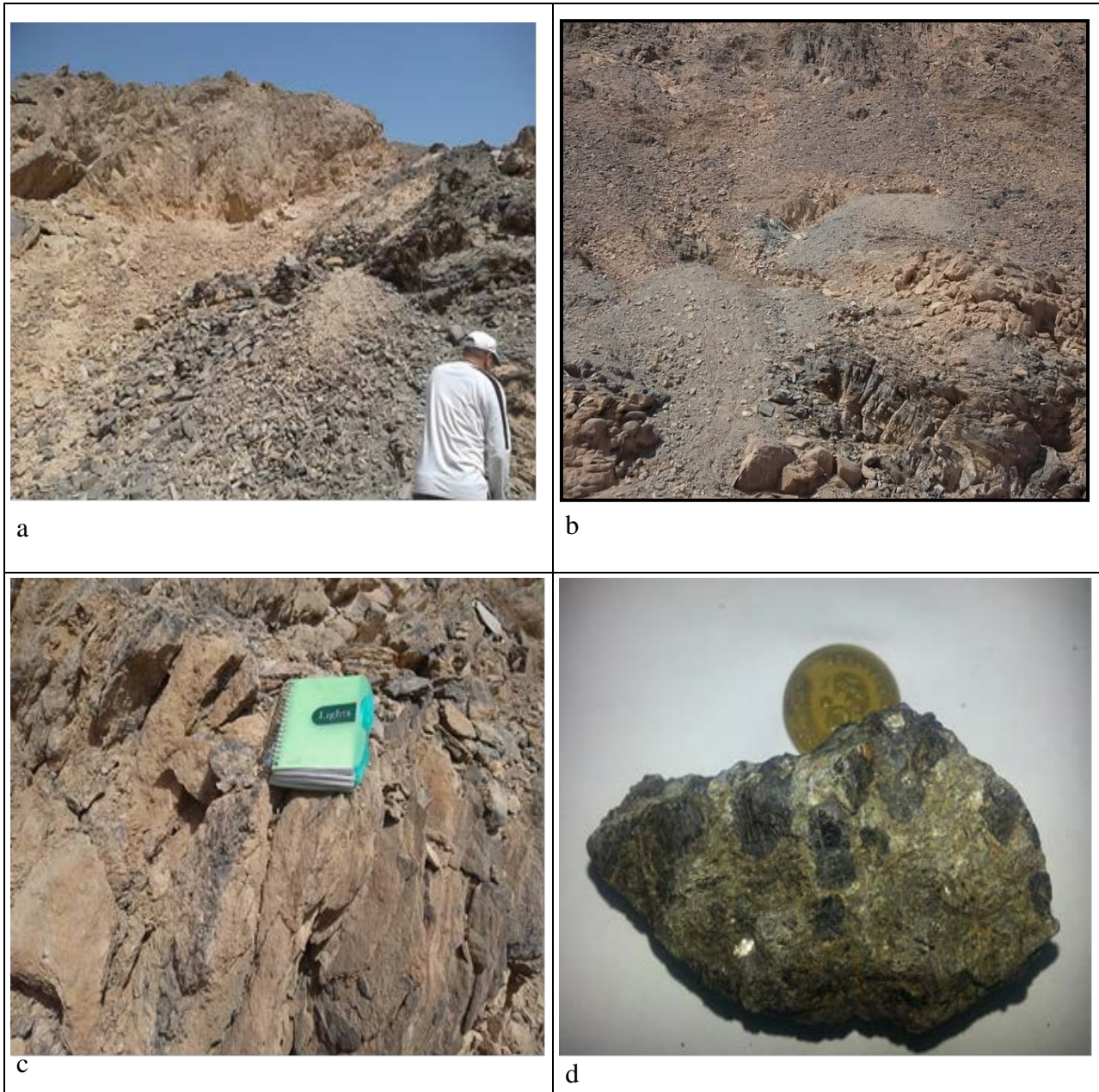


Fig.3. Photographs showing the field relationship of the study tourmaline bearing schists.
 a. Muscovite granites intruded within tourmaline-bearing mélangé schists at Wadi Um El-Debbaa (Looking NW).
 b. Mélangé schists - bearing ancient mine of beryl and tourmaline at Wadi Sikait (Looking NW).
 c. Tourmaline-bearing mélangé schists at Wadi Um El-Debbaa (Looking NW).
 d. Tourmaline minerals-bearing mélangé schists at Wadi Um El-Debbaa.

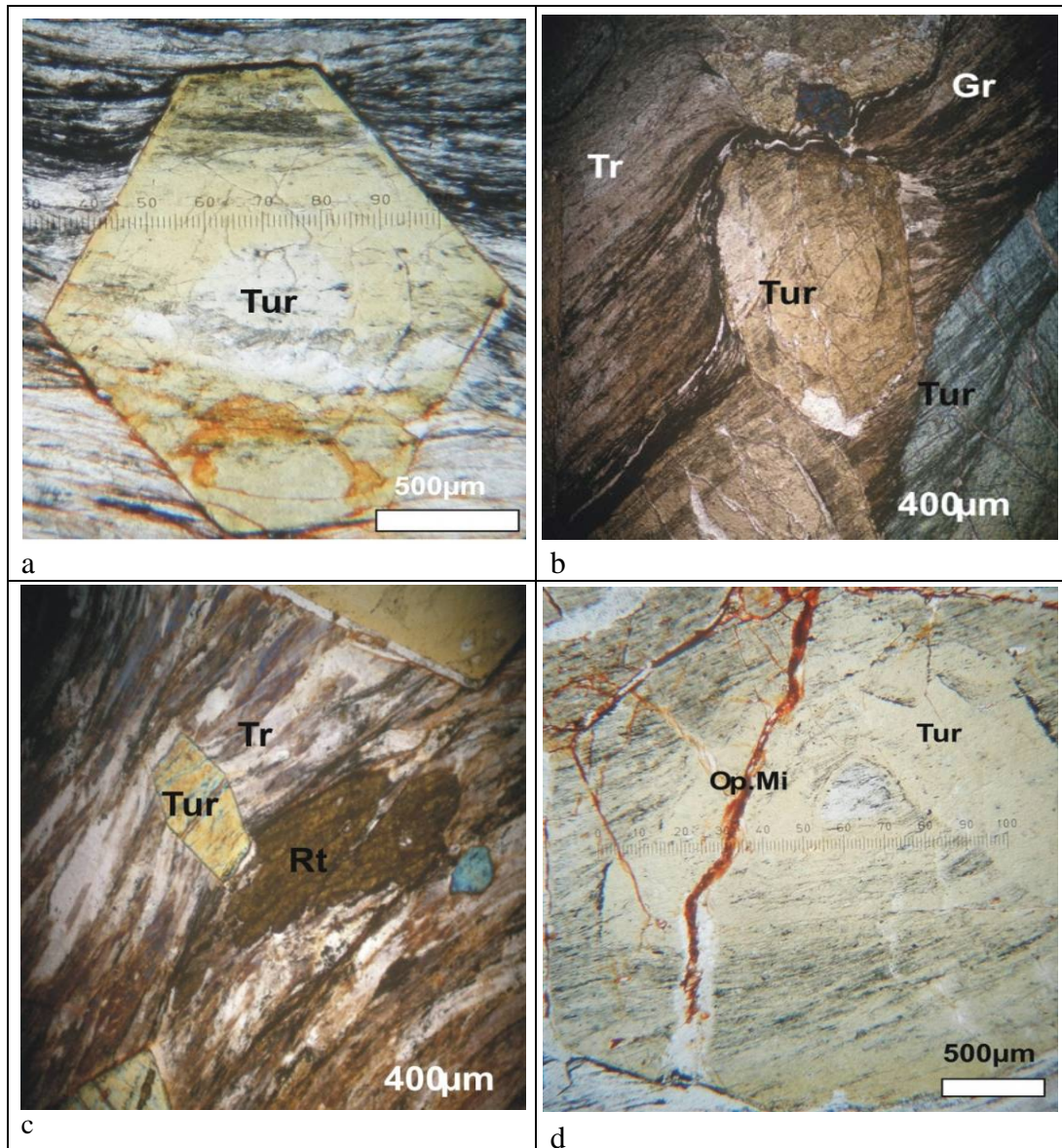


Fig.4. Photomicrographs showing some petrographical features.

- Hexagonal tourmaline (Tur) porphyroblast (CN).
- Wrapping on tourmaline (Tur) crystals (CN).
- Rutile (Rt) crystal parallel to schistosity planes (CN).
- Opaque minerals filling the fracturing of tourmaline (Tur) crystals (PPL).

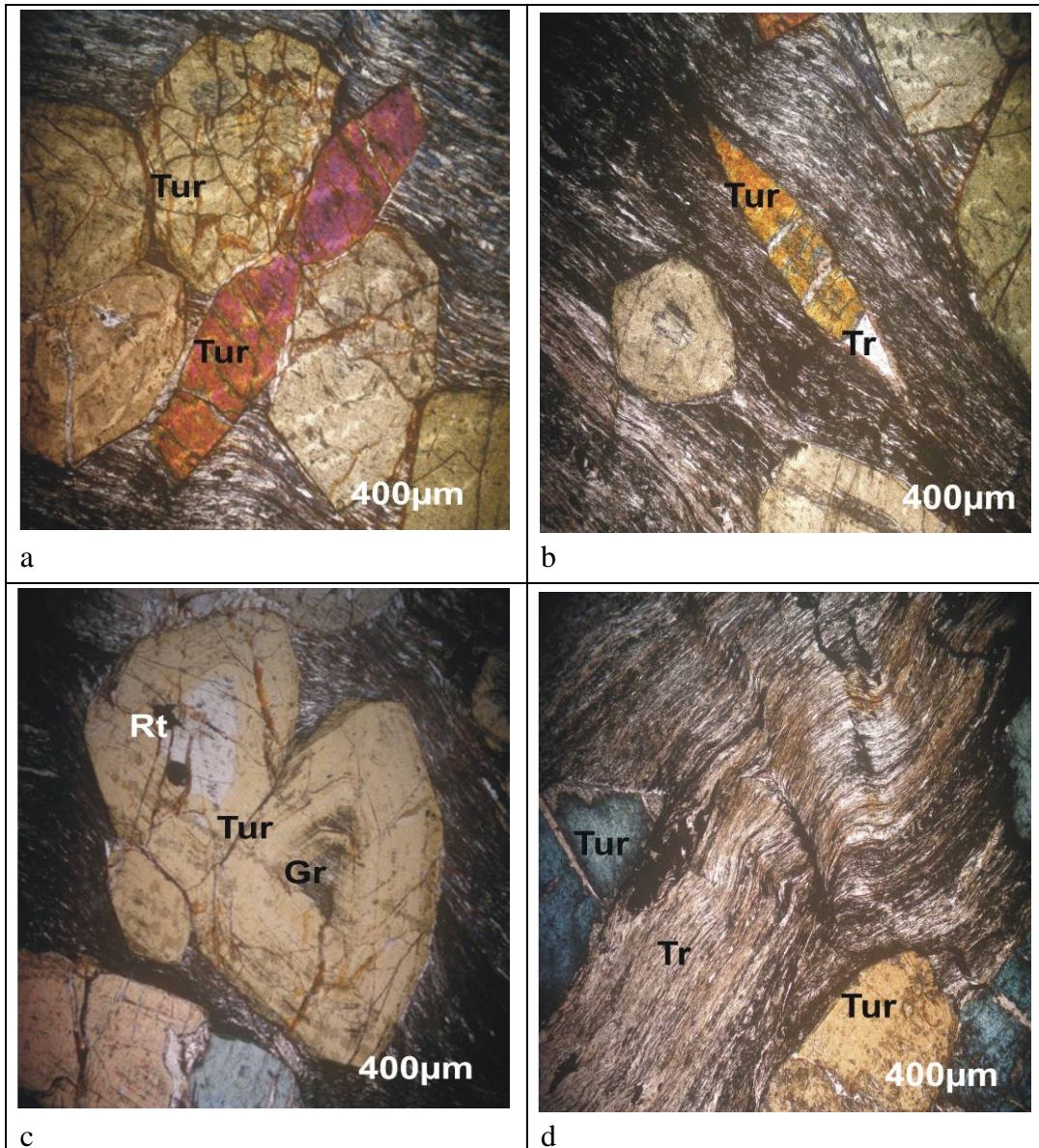


Fig.5. Photomicrographs showing some petrographical features.
a. Toothed shape of tourmaline crystal parallel to the schistosity (CN).
b. Pressure has done the teeth of tourmaline (Tur) crystals (CN).
c. Graphite in the center of tourmaline (Tur) porphyroblasts (CN).
d. Kink bands of tremolite (Tr) and opaque minerals crystals (CN).

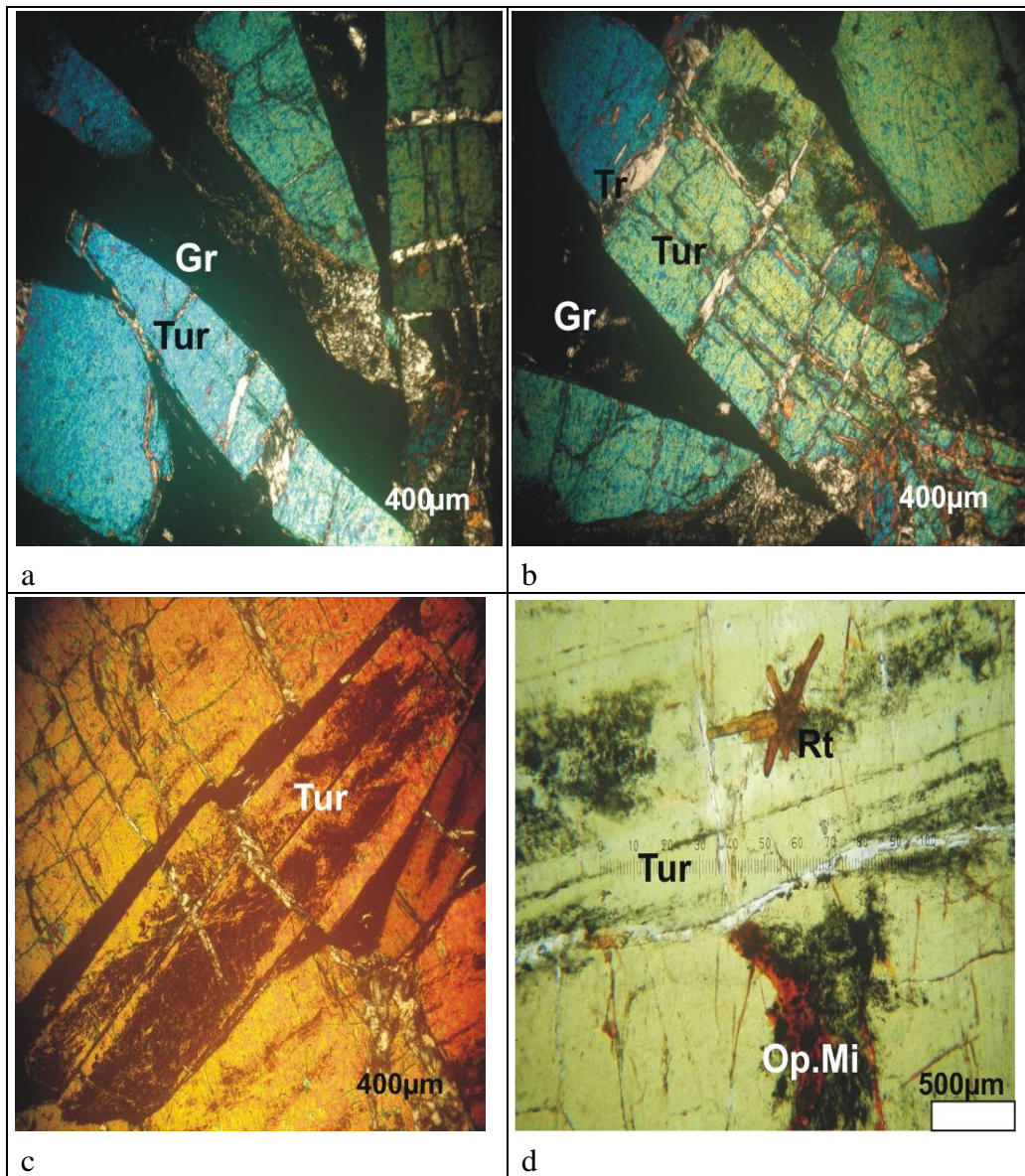


Fig.6. Photomicrographs showing some petrographical features.
 a. Tremolite (Tr) overgrowth within the fractures of tourmaline crystals (CN).
 b. Large porphyroblasts of tourmaline crystals (Tur; CN).
 c. Microfaulting within tourmaline (Tur) crystal due to micro displacement (CN).
 d. Secondary rutile (Rt) and opaque minerals (Op. Mi) filling large porphyroblast of tourmaline (Tur; CN).

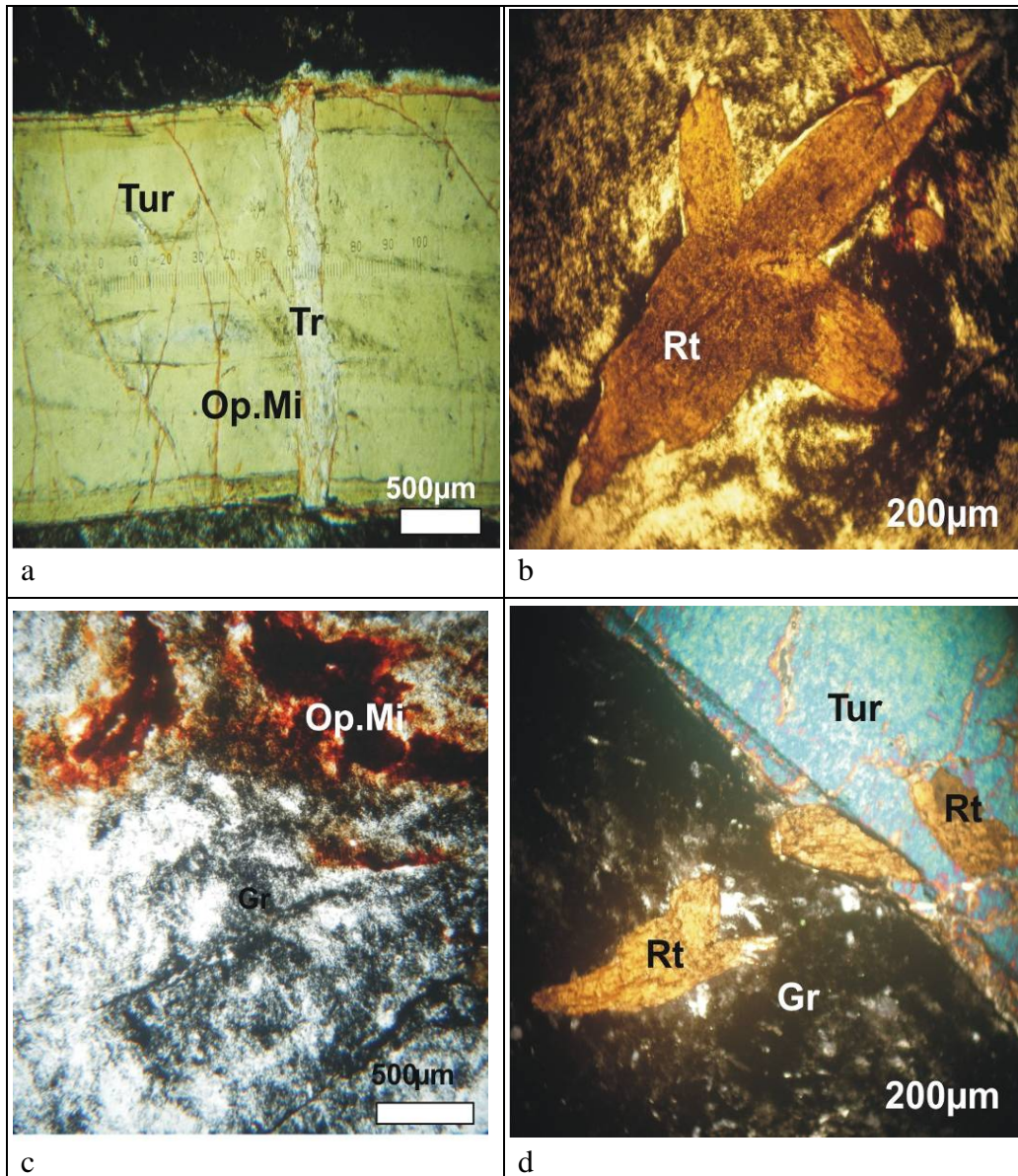


Fig.7. Photomicrographs showing some petrographical features.
 a. Prismatic crystal from tourmaline (Tur) with fracture from tremolite (Tr) and iron oxides (Op.Mi) (CN).
 b. Sphenoidal shape and growth of rutile crystals (Rt; CN).
 c. Opaque minerals (Op. Mi) incorporated within graphite (CN).
 d. Rutile crystal enclosed in tourmaline crystal (CN).

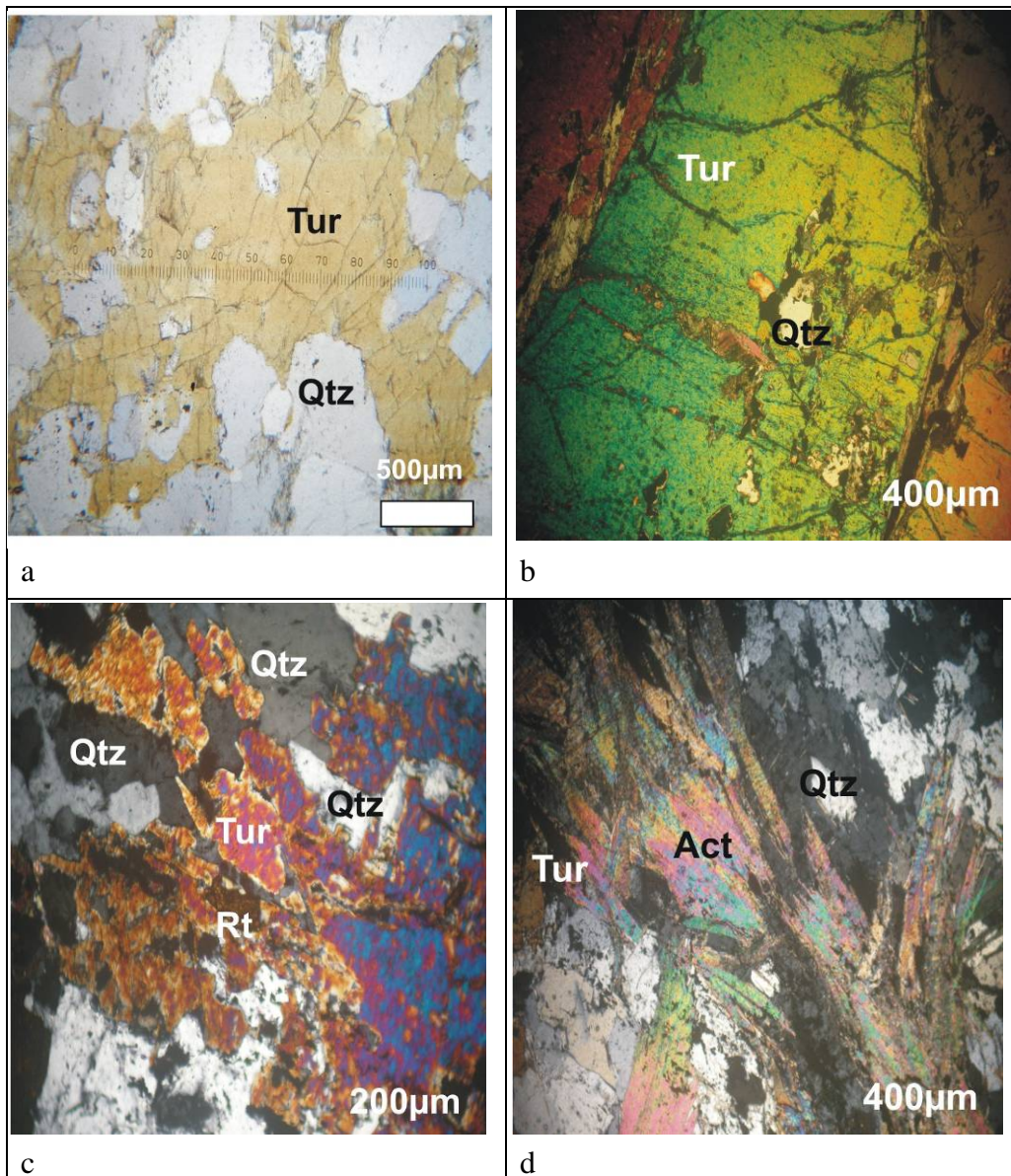


Fig.8. Photomicrographs showing some petrographical features.
 a. Quartz (Qtz) crystal enclosed in porphyroblasts of tourmaline (Tur; CN).
 b. Disseminated crystals of tourmaline (CN).
 c. Actinolite crystals led to reduce the proportion of magnesium in tourmaline (CN).
 d. Immature crystals of tourmaline because of the presence of quartz crystals (CN).

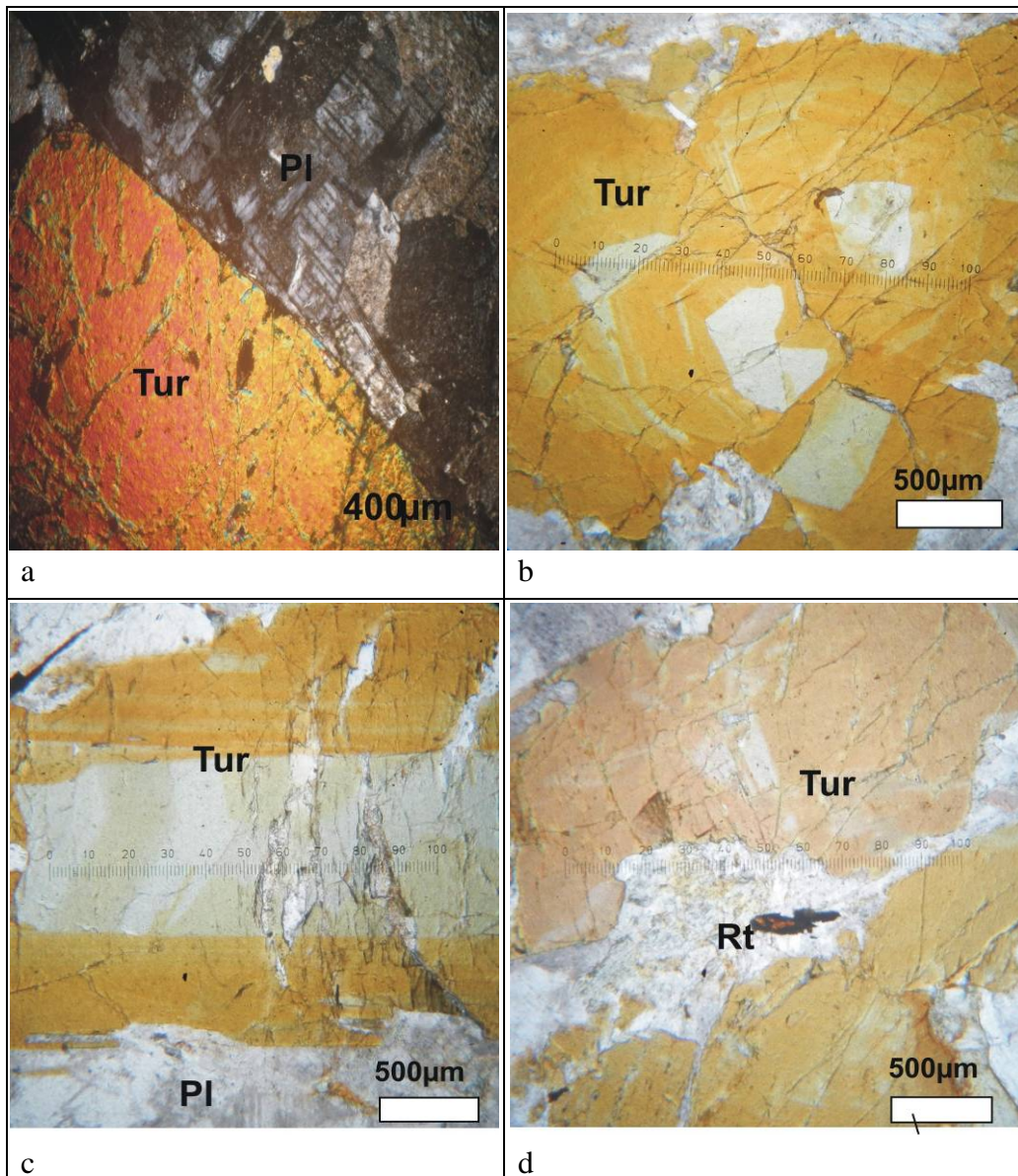


Fig.9. Photomicrographs showing some petrographical features.
 a. Mega crystal of tourmaline (Tur) with plagioclase (Pl; CN).
 b. Deformed zone of tourmaline (Tur; CN).
 c. Zonation in tourmaline (Tur) crystal (CN).
 d. Rutile crystal enclosed in tourmaline (Tur) crystal (CN).

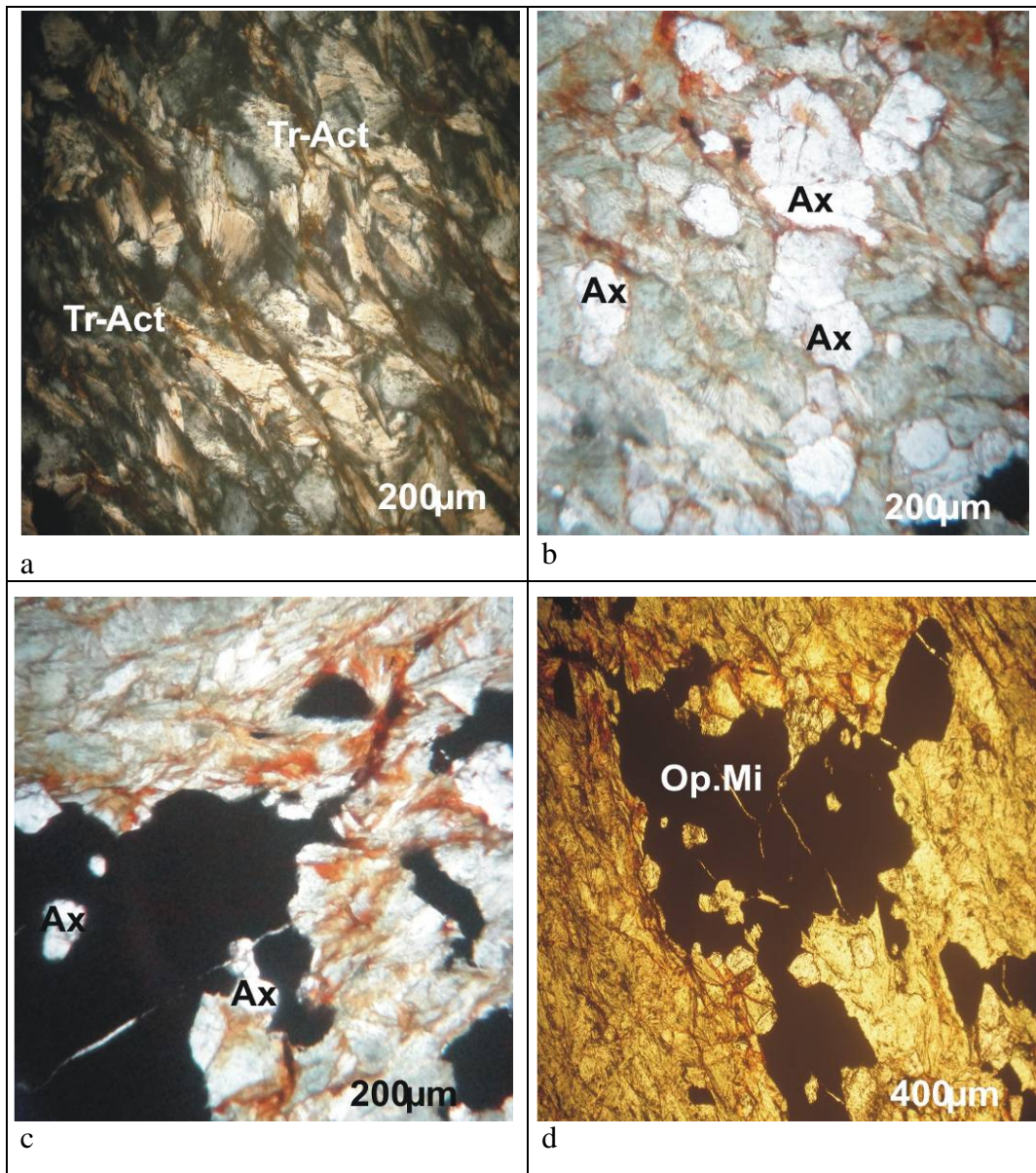


Fig.10. Photomicrographs showing some petrographical features.
 a. Green, fine-grained, acicular and prismatic tremolite and actinolite (Tr-Act) crystals well oriented with the foliation trend (CN).
 b. Medium grained high relief of axinite (Ax, CN).
 c. Axinite (Ax) crystals enclosed in iron oxides (CN).
 d. Granular crystals of iron oxides (Op. Mi; CN).

4.2. Modal composition of tourmaline-bearing schists

Because of the metamorphic overprint, it is not always possible to use conventional sedimentary or igneous rock names. Clues to the original protoliths include relict bedding and rare recognizable rock fragments in the sedimentary rocks, and relict igneous textures in the metavolcanic rocks.

The various rocks of presumed sedimentary derivation were classified in two-step process, starting with a ternary diagram of end-members quartz + feldspar, phyllosilicates, and opaque iron oxides (Fig.11c); boundary of 20% modal iron oxides was arbitrarily chosen to separate "iron-formation" from the other sedimentary rocks. Rocks with <20% opaque iron oxide were re-plotted on a quartz-feldspar-phyllosilicate diagram (Fig.11d) and named in accordance with the classification scheme of **Pettijohn (1972)**. Recognizable rock fragments, although indicative of a sedimentary protolith, are very rare and were omitted from the classification. The present work assumed that the phyllosilicates biotite represent a recrystallized pelitic matrix. The plotted tourmaline-bearing schists referred to as feldspathic arenite and greywacke (Fig.11d).

4.3. Chemical composition classes of the tourmaline-bearing schists and their protoliths

On the $\text{MgO-Fe}_2\text{O}_3\text{-Al}_2\text{O}_3$ ternary diagram (Fig.12a) proposed by **Nockolds (1947)** to distinguish between igneous and metamorphic protoliths, all samples fall in the metamorphic field. Figure (12b) shows the relationship between TiO_2 and SiO_2 as proposed by **Tarney (1976)**, with a dividing line distinguish between the metasediments and meta-igneous protoliths. The plots of the investigated samples fall in the metasediments and meta-igneous fields.

The groups of tourmaline-bearing schists seem to be good crystalline boron-rich schists. Tourmaline-bearing schists in Wadi El-Gemal more closely resemble siliceous and aluminous rocks, with the only difference being enrichment in boron. Their genesis may be revealed using the TiO_2 , Al_2O_3 , and Na_2O contents of siliceous rocks. On $\text{TiO}_2\text{-Al}_2\text{O}_3$ and $\text{Al}_2\text{O}_3\text{-(K}_2\text{O} + \text{Na}_2\text{O)}$ binary diagrams (Figs.12c & d), the dashed line effectively separates siliceous rocks of biogenic sedimentary origin and those of submarine-hydrothermal origin. Below the dashed line is the field of biogenic siliceous rocks. The data points for siliceous rocks in Wadi El-Gemal fall in the same field as those for siliceous rocks from volcanic arcs, siliceous rocks deposited from submarine hydrothermal brines (**Han Fa and Hutchinson 1989**). The analyses for the Wadi El-Gemal tourmaline-bearing schists are considered to be a base-metal massive sulfide deposit formed by submarine exhalation (**Hamilton et al., 1982**).

Table 1. Major oxide contents (wt %) of the tourmaline-bearing schists.

Oxides	Um El-Debbaa						Um Slimite					
	1D	2D	3D	4D	5D	6D	7S	8S	9S	10S	11S	12S
SiO ₂	66.70	65.70	64.98	68.10	67.71	66.40	65.10	64.77	65.10	61.88	62.66	62.40
TiO ₂	0.5	0.27	0.90	0.64	0.70	0.59	0.44	0.72	0.42	0.82	0.79	0.89
Al ₂ O ₃	15.99	15.10	16.02	14.23	15.72	15.88	15.71	14.83	14.59	17.62	16.69	16.72
Fe ₂ O ₃	2.35	3.04	3.21	2.87	3.05	3.27	2.81	3.22	3.27	3.74	3.80	3.45
FeO	2.12	2.73	2.89	2.58	2.74	2.95	2.53	2.90	2.94	3.37	3.42	3.11
MnO	0.03	0.06	0.05	0.11	0.09	0.08	0.02	0.09	0.07	0.03	0.02	0.04
MgO	4.13	4.90	5.01	5.23	4.36	4.39	4.82	5.19	6.10	2.87	3.52	3.59
CaO	0.83	0.79	1.02	0.54	0.73	0.86	1.14	0.45	0.62	1.66	0.96	1.32
Na ₂ O	2.40	1.97	2.11	2.09	1.57	1.39	1.57	2.04	2.09	1.22	1.95	1.87
K ₂ O	1.34	3.13	2.06	1.24	1.37	2.06	2.19	2.72	2.65	3.11	3.02	2.97
P ₂ O ₅	0.22	0.19	0.15	0.09	0.07	1.01	0.37	0.42	0.59	0.32	0.28	0.25
LOI	2.99	2.11	2.46	1.79	2.42	1.09	2.72	2.01	2.07	2.36	2.45	3.02
Total	99.60	99.98	100.86	99.51	100.53	99.97	99.42	99.36	100.51	99.00	99.56	99.63
Na ₂ O/ K ₂ O	1.79	0.63	1.02	1.69	1.15	0.67	0.72	0.75	0.79	0.39	0.65	0.63

Table 1. Continued.

Oxides	Wadi Abu Rusheid						Wadi Sikait					
	13R	14R	15R	16R	17R	18R	19K	20K	21K	22K	23K	24K
SiO ₂	61.92	64.99	63.75	62.96	63.62	65.25	63.98	63.79	62.2	60.95	62.12	63.19
TiO ₂	0.92	0.83	0.72	0.65	0.77	0.82	0.96	0.79	0.72	0.83	0.69	0.89
Al ₂ O ₃	16.89	16.85	15.96	16.75	17.24	17.09	17.18	16.85	18.12	17.19	17.59	18.36
Fe ₂ O ₃	4.06	3.45	3.57	3.70	3.40	3.56	3.68	3.74	3.24	3.78	2.82	3.05
FeO	3.66	3.10	3.22	3.32	3.05	3.21	3.31	3.36	2.92	3.41	2.54	2.74
MnO	0.05	0.03	0.03	0.04	0.02	0.06	0.05	0.04	0.05	0.02	0.03	0.04
MgO	3.29	2.72	3.39	2.86	2.79	2.66	3.22	3.01	2.7	2.89	3.11	2.82
CaO	0.72	1.26	1.56	1.45	0.96	0.86	0.88	0.92	0.92	1.07	1.34	0.86
Na ₂ O	1.75	2.11	2.02	2.36	2.32	1.97	1.84	2.03	2.10	2.36	2.75	1.89
K ₂ O	3.09	2.09	3.19	3.27	2.49	2.1	2.32	3.02	2.80	3.11	3.26	2.72
P ₂ O ₅	0.24	0.29	0.12	0.19	0.36	0.26	0.18	0.27	0.42	0.32	0.27	0.42
LOI	2.67	1.79	2.29	2.1	2.72	1.87	2.92	2.01	3.23	3.10	2.85	2.15
Total	99.26	99.51	99.91	99.65	99.74	99.71	100.52	99.83	99.42	99.03	99.37	99.13
Na ₂ O/ K ₂ O	0.57	1.01	0.63	0.72	0.93	0.94	0.79	0.67	0.75	0.76	0.84	0.69

Table 2. Trace elements contents (ppm) of the tourmaline-bearing schists.

Elements	Um El Debbaa						Um Slimata					
	1D	2D	3D	4D	5D	6D	7S	8S	9S	10S	11S	12S
Cr	381	297	245	280	724	689	144	164	147	160	145	61
Ni	245	142	124	138	225	202	158	114	138	129	113	111
Cu	11	11	18	12	13	9	10	8	8	9	7	8
Zn	107	87	88	89	89	71	109	137	98	107	105	87
Zr	291	445	464	420	248	182	169	68	124	153	113	253
Rb	17	16	24	27	12	12	576	702	433	604	677	595
Y	109	162	173	153	96	74	73	34	53	70	49	109
Ba	79	132	153	131	64	60	67	60	57	73	63	59
Pb	45	70	77	81	27	68	37	36	25	33	26	32
Sr	305	471	487	450	251	179	128	24	92	118	65	221
Ga	13	19	27	17	8	16	6	12	6	14	4	15
V	261	414	452	438	230	215	193	170	173	199	176	185
Nb	459	690	730	666	393	295	269	103	198	257	172	416
B	1120	710	1410	1820	920	2140	240	410	230	350	245	510
U	2	-	3	-	-	2	-	-	2	2	3	2
Th	9	8	11	4	3	7	2	4	6	5	7	5
Rb/Sr	0.06	0.03	0.05	0.06	0.05	0.07	4.5	29.25	4.71	5.12	10.42	2.96
Zn/(Pb+Zn)	0.70	0.55	0.53	0.52	0.77	0.51	0.75	0.79	0.80	0.76	0.80	0.73

Table 2. Continued

Elements	Wadi Abu Rusheid						Wadi Sikait					
	13R	14R	15R	16R	17R	18R	19K	20K	21K	22K	23K	24K
Cr	283	289	121	1168	1157	1263	940	998	1146	748	873	1150
Ni	164	200	265	834	553	660	558	784	1065	498	509	614
Cu	15	18	13	29	31	36	7	9	9	20	10	8
Zn	1230	1292	692	4326	3503	2849	92	135	102	167	108	107
Zr	277	268	477	185	111	105	123	142	139	197	165	108
Rb	258	365	1002	1276	1518	1134	64	100	110	52	147	108
Y	128	122	219	87	60	50	58	68	63	74	76	52
Ba	62	65	103	44	43	34	44	48	45	51	48	47
Pb	439	538	417	864	999	1465	12	18	15	84	13	12
Sr	242	233	396	98	19	30	121	128	118	195	150	88
Ga	131	165	123	264	345	489	-	3	-	28	6	4
V	175	185	219	143	139	109	152	160	156	272	157	157
Nb	455	437	788	293	181	165	207	231	228	301	267	175
B	1120	865	1045	1285	875	1244	550	790	485	630	370	586
U	3	4	3	5	5	4	-	2	2	-	2	2
Th	10	12	12	15	17	13	4	5	3	4	5	4
Rb/Sr	1.07	1.57	2.53	13.02	79.89	37.8	0.53	0.78	0.93	0.27	0.98	1.23
Zn/(Pb+Zn)	0.74	0.75	0.62	0.83	0.78	0.66	0.88	0.88	0.87	0.67	0.89	0.90

Table 3. Rare earth elements of the studied tourmaline-bearing schists.

Elements	Um El-Debbaa			Um Slimat			Wadi Abu Rusheid			Wadi Sikait		
	1D	3D	6D	1S	4S	6S	2R	4R	6R	1K	3K	6K
La	19.77	18.1	21.11	22.3	17.1	18.76	23.11	25.55	14.16	17.11	21.15	16.26
Ce	30.16	36.1	39.56	41.26	43.76	47.21	32.98	29.27	30.66	38.12	43.67	35.79
Pr	5.9	5.75	6.77	6.18	6.35	6.92	5.61	5.29	5.59	5.71	5.46	5.34
Nd	15.66	14.1	13.29	15.87	18.09	14.72	19.11	20.01	15.12	16.91	17.02	16.56
Sm	3.97	4.02	4.12	3.67	4.65	5.11	5.02	3.98	3.82	2.97	4.15	4.05
Eu	1.01	0.97	0.86	1.12	1.09	0.79	0.8	1.08	1.17	1.25	0.92	1.15
Gd	3.97	4.01	4.42	3.8	3.56	3.42	4.75	4.19	4.36	4.62	4.12	4.22
Tb	0.72	0.66	0.62	0.59	0.45	0.63	0.82	0.89	0.79	0.69	0.72	0.69
Dy	2.44	3.09	4.02	4.12	3.86	2.72	2.15	2.39	2.42	3.45	3.25	3.11
Ho	0.64	0.75	0.92	0.86	0.69	0.73	0.62	0.59	0.67	0.83	0.97	0.75
Er	2.1	2.71	2.88	2.65	2.55	2.17	2.69	2.77	2.95	2.63	2.45	2.65
Tm	1.98	1.01	1.45	1.33	0.99	1.11	2.63	2.22	2.15	2.44	2.03	2.04
Yb	2.32	2.45	2.72	2.82	2.88	2.09	3.01	2.89	2.97	2.87	2.68	2.49
Lu	0.32	0.46	0.52	0.59	0.61	0.34	0.39	0.49	0.59	0.47	0.35	0.31

4.4. Tectonic setting of protoliths for tourmaline-bearing schists

On the $\text{TiO}_2\text{-K}_2\text{O-P}_2\text{O}_5$ ternary diagram (Fig.13a), suggested by **Pearce et al. (1975)** to differentiate between continental and oceanic tectonic setting, all the analyzed samples are plotted in continental setting along $\text{TiO}_2\text{-K}_2\text{O}$ side.

Bhatia (1983) used the plots of $(\text{Fe}_2\text{O}_3^{\text{t}} + \text{MgO})$ versus TiO_2 (Fig.13b) to discriminate between four types of settings: A-oceanic island arc (e.g. Marianas and Aleutians), B-continental island arc (e.g. Japan Sea and Cascades), C-active continental margin (Andean type) and D-passive margin. The plotted samples fall within or close to the fields of continental island arc (B) and active continental margin (C) sandstones. **Bhatia (1983)** mentioned that continental island arcs or island arcs partly formed on thin continental crust are sedimentary basins adjacent to the oceanic island arcs. This gives an explanation to the sample plotted in the island arc field.

Three tectonic settings of the passive continental margin (PM), the active continental margin (ACM) and the oceanic island arc are recognized on the $\text{K}_2\text{O/Na}_2\text{O}$ versus SiO_2 discrimination diagram (Fig.13c) of **Roser and Korsch (1986)** for sandstone-mudstone suites. The plotted samples are concentrated in the island arc schist field except one sample fall in active continental margin field.

On the $\text{FeO}^{\text{t}}\text{-MgO-Al}_2\text{O}_3$ diagram (Fig.13d) of **Pearce and Gale (1977)**, all the data points form a tight cluster and fall within field 2 (island arc and active continental margin); it is rich in Al_2O_3 contents.

4.5. Magma type of protoliths for tourmaline-bearing schists

On the alkali-silica diagram (Fig.14a) of **Irvine and Baragar (1971)**, the analyzed tourmaline-bearing schists plotted on these diagram show that they derived from sub-alkaline affinities. **Shand (1951)** reported that the $\text{Al}_2\text{O}_3 - \text{CaO} - (\text{Na}_2\text{O} + \text{K}_2\text{O})$ oxides should be most effective in distinguishing peraluminous, meta-aluminous and peralkaline magma types. The plotted samples are occupied in the peraluminous field (Fig.14b).

4.6. Chemographic system in the metamorphic conditions

The chemographic system in the metamorphic conditions could be illustrated by using the relationships between the chemical characters and metamorphic events. The relationship between the Al_2O_3 and CaO contents was used by **Aumento and Laubert (1971)** to differentiate between low and high temperatures. On their diagram (Fig.14c) the analyzed samples are encountered in low metamorphic temperature. A discrimination diagram based on the $\text{Na} + \text{K}$ and Ti contents have already been shown useful for distinguishing between greenschist facies, amphibolite facies and granulite facies (**Zakrutkin, 1968**). The data points of the present tourmaline-bearing schists on that diagram fall within the field of amphibolite facies (Fig.14d).

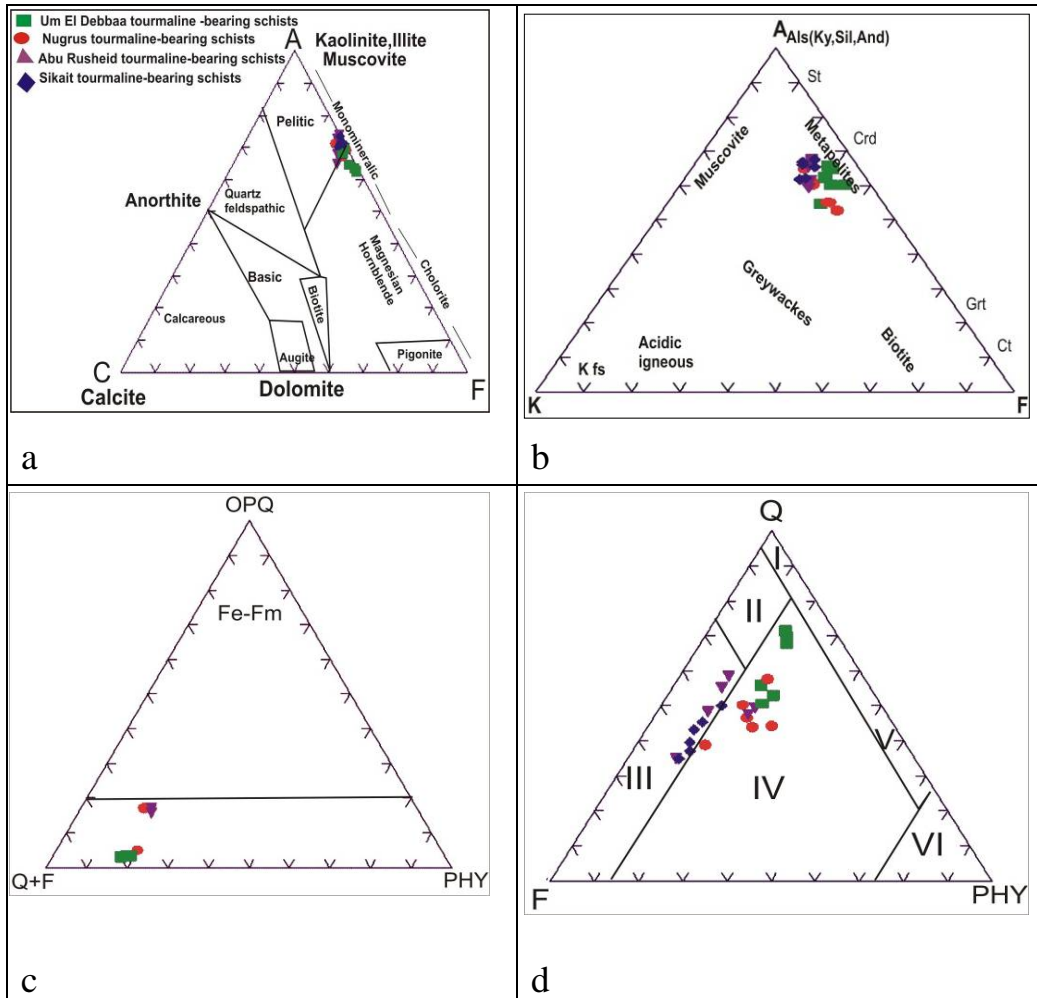


Fig.11a. ACF ternary diagram of the tourmaline-bearing schists (Fyfe *et al.*, 1958).

b. A'KF ternary diagram of the tourmaline - bearing schists (Winkler, 1976). The abbreviation of minerals by Kretz (1983).

c & d. Modal diagrams used to infer protoliths of metasedimentary rocks (Pettijohn, 1972). OPQ, opaque oxides; Q, quartz; F, feldspar; PHY, phyllonites; I, quartz arenite; II, arkose; III, feldspathic arenite; IV, feldspathic greywacke; V, greywacke; and VI, mudstone. Legend as in Fig. (11a).

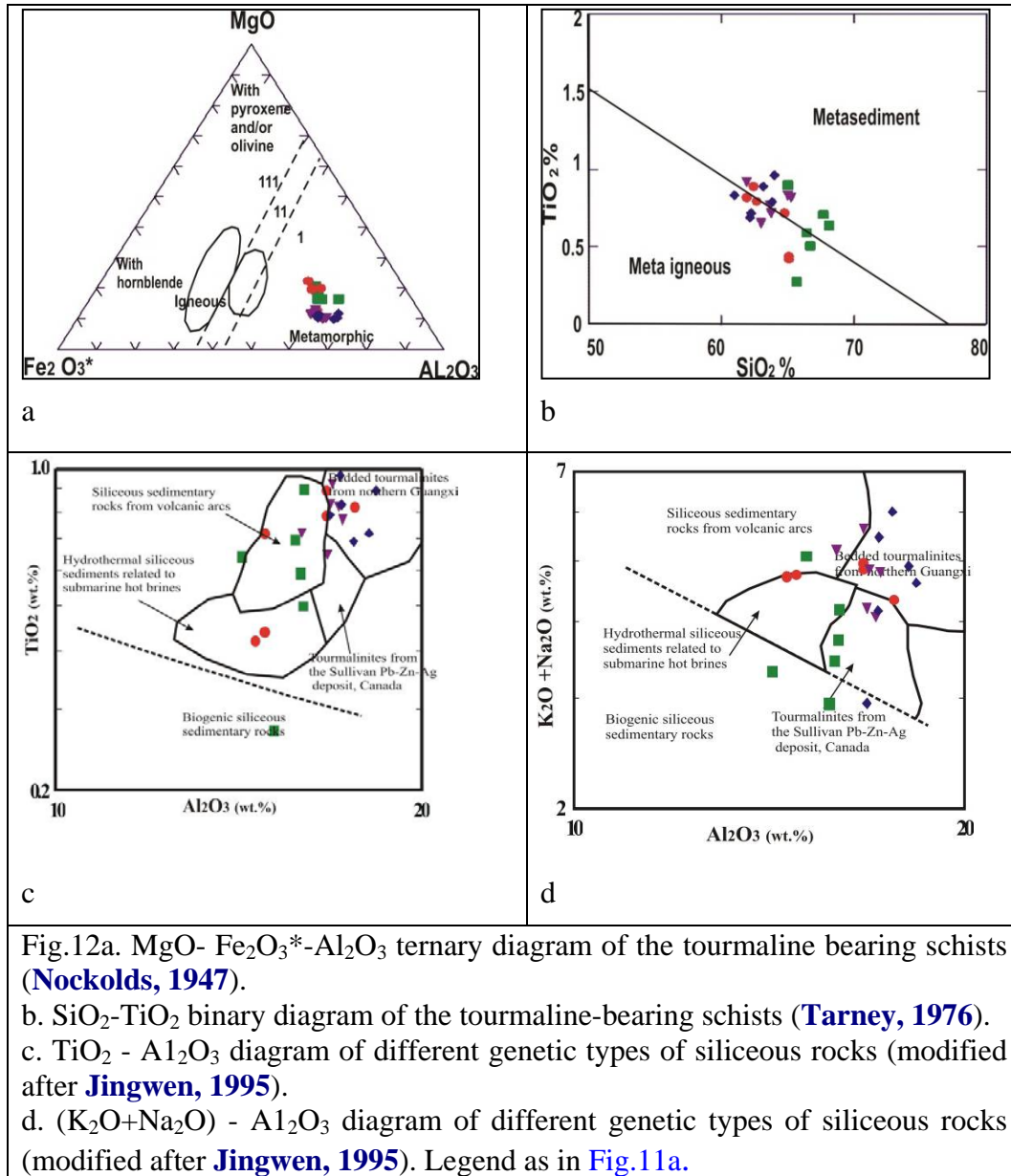
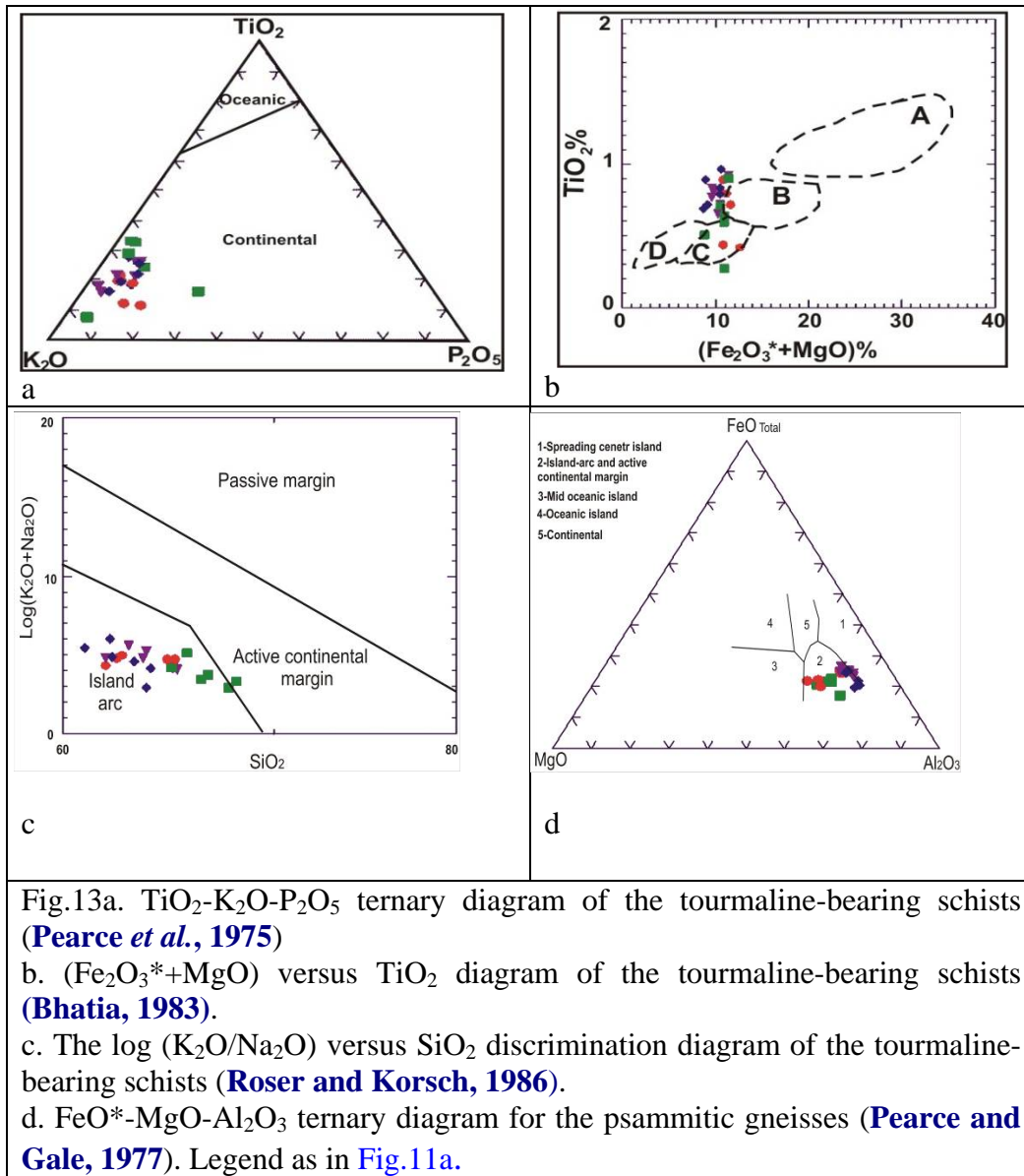
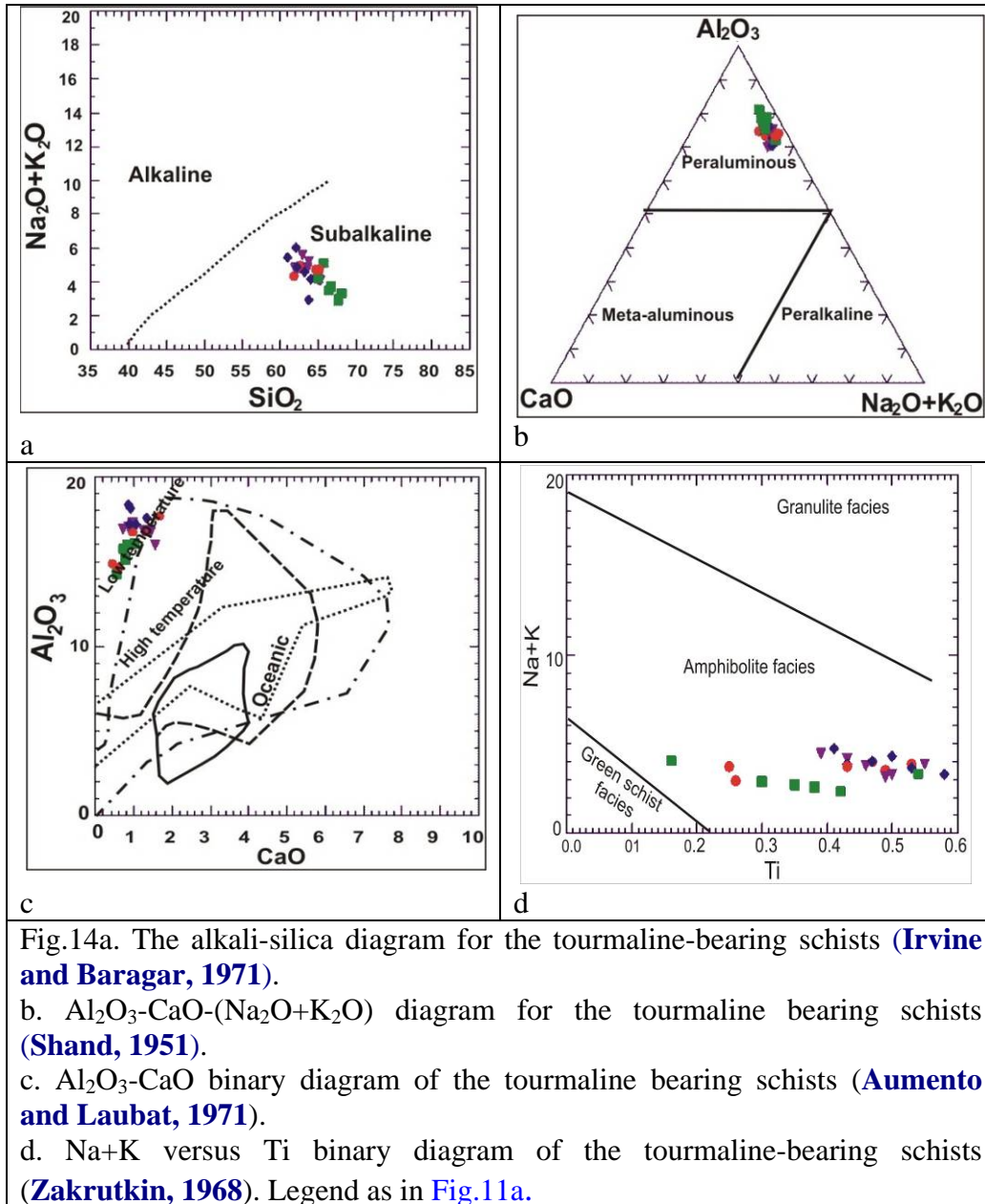


Fig.12a. MgO- Fe₂O₃*-Al₂O₃ ternary diagram of the tourmaline bearing schists (Nockolds, 1947).
 b. SiO₂-TiO₂ binary diagram of the tourmaline-bearing schists (Tarney, 1976).
 c. TiO₂ - Al₂O₃ diagram of different genetic types of siliceous rocks (modified after Jingwen, 1995).
 d. (K₂O+Na₂O) - Al₂O₃ diagram of different genetic types of siliceous rocks (modified after Jingwen, 1995). Legend as in Fig.11a.





5. Trace and REE elements geochemistry

The tourmaline-bearing schists at Wadi El-Gemal district contains different contents of trace elements, such as B, Cr, Cu, Rb, Pb, U and Th. Tourmaline-bearing schists have higher B, Cr, Zn, and Rb and medium Ni, Zr, Ba, Sr, V, and Nb and lower Cu, Ga, Y, U, and Th (Table 2).

On the Al_2O_3 - Cr and TiO_2 - Cr of variation diagram (Fig.15a & b) of Slack *et al.* (1993) and Pesquera and Velasco (1997) the Cr values exhibit a positive correlation with Al and Ti, implying a similar behavior during sedimentary and metamorphic processes. Similar to the major elements, however, some scatters in the data are observed as a result of metasomatic changes of relatively immobile trace elements, such as Cr and Ti, the tourmaline-bearing schists on average have higher Cr, TiO_2 and Al_2O_3 at Wadi El-Gemal district (Fig.15a & b). This relative increase in the whole rock concentration of the low solubility elements Al, Ti and Cr may result from residual enrichment caused by the removal of the other more soluble species during tourmalinization and regional metamorphism (Harraz and El-Sharkawy, 2001).

On the Y - Yb and Y - Lu binary diagrams of Slack *et al.* (1993), the greater scatter in the data for tourmalinites is probably due to some mobility of the light REE (LREE), relative to Th, during the formation of the tourmaline-rich rocks (Slack *et al.*, 1993). By contrast, the heavy REE (HREE) do not appear to have been significantly mobile during hydrothermal and metamorphic processes, as evidenced by correlations between Yb - Y and Lu - Y (Fig.15c & d).

The trace elements distribution (chondrite normalized; Thompson, 1982) of the tourmaline-bearing schists in three different patterns can be observed, the most samples are of enrichment patterns and low samples are of depleted patterns (Fig.16).

The chondrite-normalized REE patterns of the tourmaline-bearing schists are characterized by a depletion of HREE relative to LREE and negative Eu and Ce anomalies (Fig.17). The average chondrite-normalized patterns are commensurate to those of metapelitic rocks elsewhere. In addition they are having negative Eu anomalies, and appear to be of typical upper continental crust (McLennan, 1989).

The negative Ce anomalies of the tourmalinites are very similar to those of tourmaline-rich rocks in the Broken Hill district, Australia (Lottermoser, 1989; Slack *et al.*, 1993). Moreover, the negative Ce anomalies of the tourmalinites are very similar to those of modern ferromanganese nodules and associated sediments of the Pacific Ocean (Eiderfield *et al.*, 1981), suggesting that the sea water-derived fluid was involved in the initial formation of the tourmalinites. The negative Eu anomaly is interpreted as typical for the formation of the tourmalines and their host schists in an upper Proterozoic metasedimentary environment (Mohamed and Hassanen, 1997).

Differences in the Y and REE abundances, relative to the general trend for some tourmalinites, suggest that REE distributions may have been controlled mainly by the hydrothermal fluids (King *et al.*, 1988). Low contents of REE may indicate that tourmalinites are formed from colloids or gels (Slack, 1996).

The chondrite-normalized REE patterns (Fig.17) suggested that the tourmaline and their host-rock metapelites were formed in a submarine environment. However, the low Fe/Al ratios of the tourmaline-bearing schists in the studied areas are different from the high Fe/Al ratios of submarine hydrothermal fluids sampled from active sea-floor vents (e.g. Von Damm *et al.*, 1985). In evaluating this point, Slack *et al.* (1993) proposed that because tourmaline has low

Fe/Al ratios, an exhalative fluid would be undersaturated with respect to tourmaline away from the vents, and would be unable to precipitate tourmaline directly from solution.

6. Tourmaline composition versus rock type

Tourmaline crystals from facies correlated with volcanosedimentary protoliths are essentially dravitic showing Mg enrichment and Na depletion. Porphyroblastic tremolite, typical of the regional essentially of pelitic formation, in the tourmaline horizons leads to porphyroblastic axinite with the same kinematic niche. The two minerals are equivalent to the same thermotectonic conditioning. [Figure \(18a\)](#) shows tourmaline compositions in the Al-Fe₅₀Al₅₀-Mg₅₀Al₅₀ diagram defined by [Henry and Guidotti \(1985\)](#). On the ternary diagram of [Henry and Guidotti \(1985\)](#), the analyzed tourmalines in the tourmaline-bearing schists plot predominantly within the host rock field described as Fe³⁺-rich quartz-tourmaline rocks, calc-silicate rocks, and metapelites (Field 6), and in the field of Fe³⁺-rich quartz-tourmaline rocks (hydrothermally altered granites, field 3).

On the Ca-Fe-Mg plot ([Fig.18b](#)), the tourmalines in the tourmaline-bearing schists, plots are between the fields described as Li-rich granitoid pegmatites and aplites (Field 1), Li-poor granitic rocks (Field 2) and Ca-poor metapelites, metapsammites, and quartz-tourmaline rocks (Field 8).

In [Figure 18c](#), the tourmalines in the variety of tourmaline-bearing schists fall in the fields that suggest the tourmalines formed in relatively Li-rich granitoid pegmatites and aplites (field 1), Li-poor granitoids and their associated pegmatites and aplites (field 2), metapelites and metapsammites coexisting with an Al-saturating phase, (field 4, probably with graphite present). The higher Ti contents imply that they formed at a different P, T condition and/or with a different Ti-saturating phase (such as rutile).

The tourmalines analyzed from the studied Wadi El-Gemal district fall roughly equally between the dravite (Mg-rich) and schorl (Fe-rich) end members, with no significant uvite or feruvite component ([Fig.18d](#)). Despite the large number of permissible substitutions, some generalizations can be made about the relationship between tourmaline composition and host rock type. Tourmaline compositions from various rock types are plotted on Al-Fe(tot)-Mg and Ca-Fe(tot)-Mg ternary diagrams, several distinct regions can be defined for tourmalines from different rock types ([Fig.18a & b](#)). Some imprecision in locating boundaries between rock types results from tourmaline-bearing schist analyses which were performed on mineral separates representing the bulk composition of tourmalines.

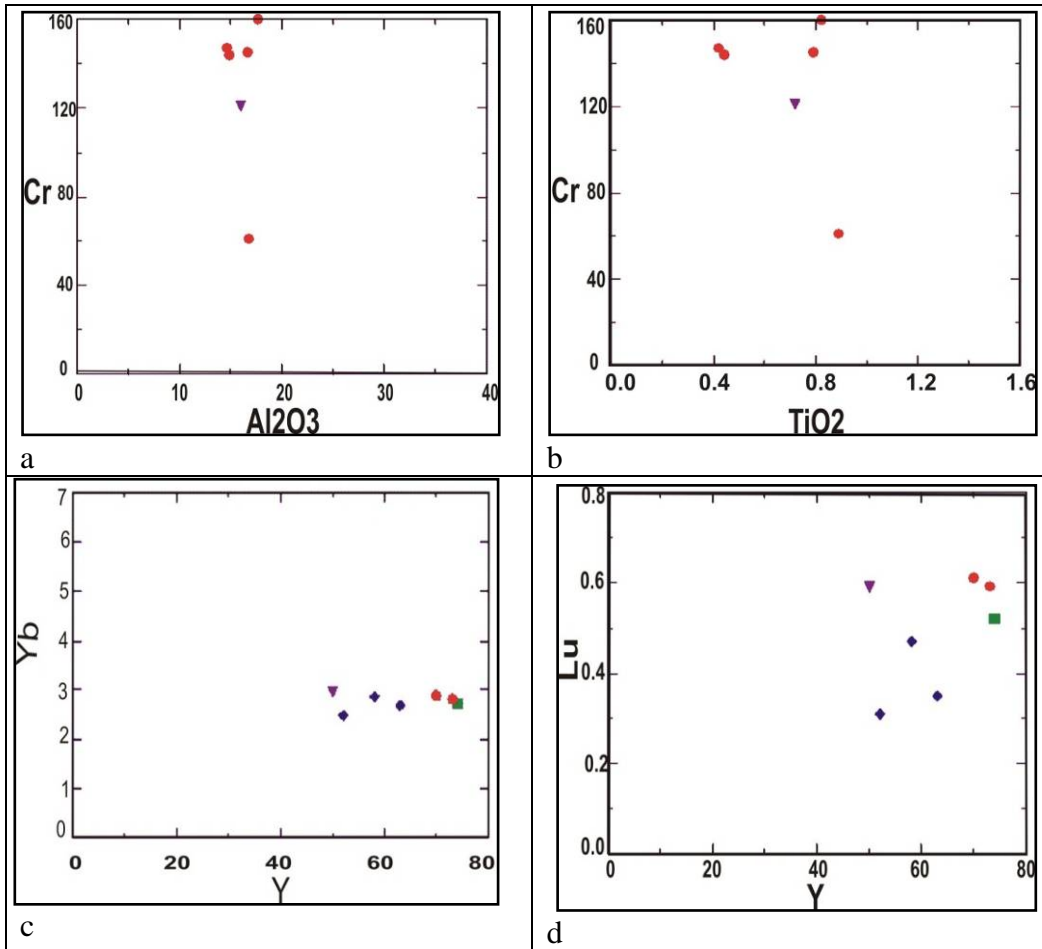


Fig.15a. Plots of Al₂O₃ - Cr diagram of the tourmaline bearing schists (Slack *et al.*, 1993; Pesquera and Velasco, 1997).
b. Plots of TiO₂ - Cr diagram for the tourmaline bearing schists (Slack *et al.*, 1993; Pesquera and Velasco, 1997).
b. Plots of Y - Yb diagram for the tourmaline bearing schists (Slack *et al.*, 1993).
c. Plots of Y versus Lu diagram for the tourmaline bearing schists (Slack *et al.*, 1993). Legend as in Fig.11a.

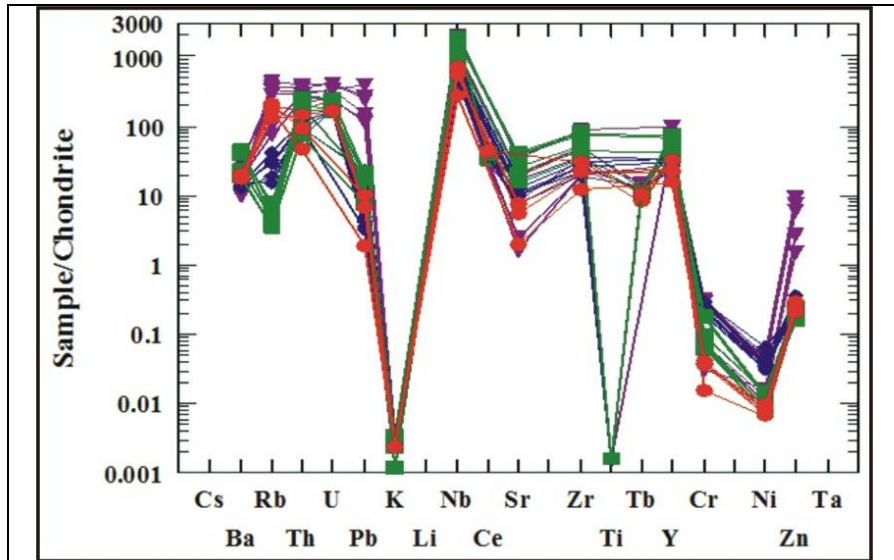


Fig.16. Trace element concentrations normalized to the composition of the tourmaline bearing schists and plotted from left to right in order of increasing compatibility in a small fraction melt of the chondritic values (The normalization values are those of **Thompson, 1982**). Legend as in Fig.11a.

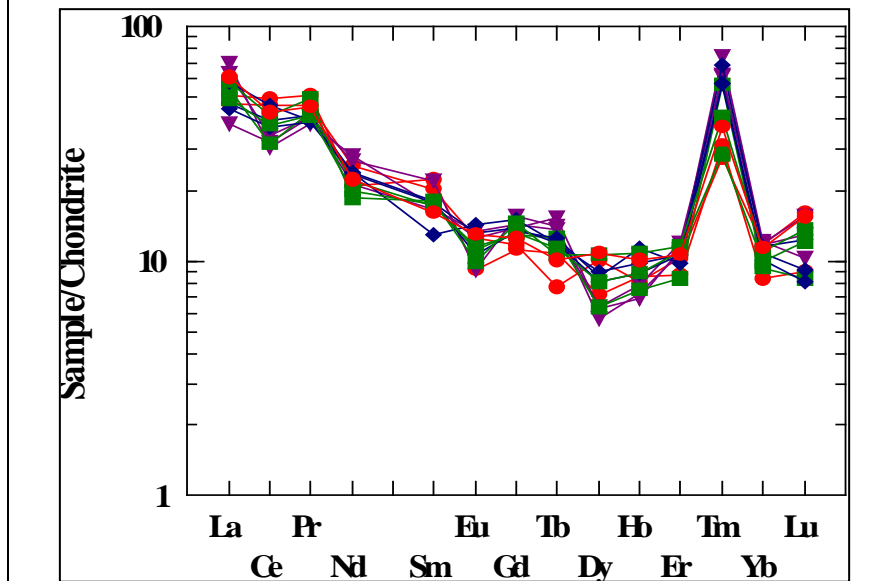
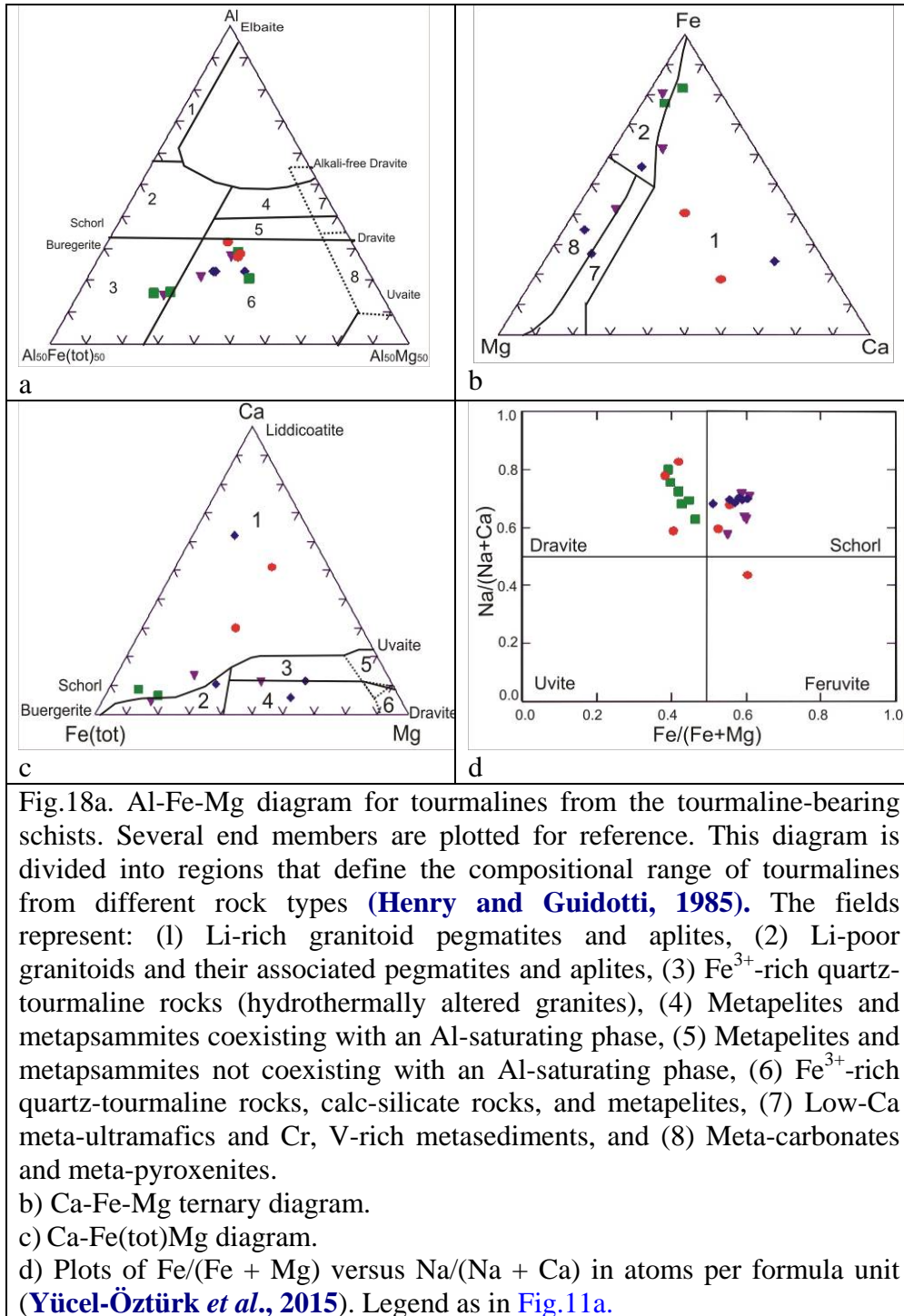


Fig.17. Chondrite-normalized REE patterns of tourmaline bearing schists according to the chondritic values of **McLennan (1989)**. Legend as in Fig.11a.



Conclusions

The tourmaline deposits hosted as zones and disseminated crystals in the tourmaline-bearing deposits at Wadi El-Gemal district which includes four areas as Um El-Debbaa (a tributary from Wadi El-Gemal), Um Slimat (a tributary from Wadi Nugrus), Wadi Sikait and Wadi Abu Rusheid. Tourmaline-bearing schists are found in arc volcanoclastic metasediments (mélange rocks). The petrographic features of the tourmaline occurrences vary, and allow its classification into seven groups, depending on the host rock lithology, mineral assemblage and their relative abundance; namely, 1) Graphite - tremolite - tourmaline schists, 2) Graphite - tourmaline - tremolite schists, 3) Graphite - tourmaline schists, 4) Tourmaline - graphite schists, 5) Tourmalinites, 6) Plagioclase - tourmaline schists, 7- Axinite-tremolite - actinolite schists. Their relative abundance varies considerably from one locality to another. The modal composition of the studied tourmaline-bearing schists) reveals that they have a wide range of mineral assemblages.

The petrochemical characteristics of the tourmaline-bearing schists are of peraluminous in nature and the source rocks originated from calc-alkaline magma. They seem to have been evolved in an island arc tectonic setting, where they are related to immature island arcs. These schists are high pressure and low temperature, amphibolite facies and kyanite zone due to regional metamorphism.

REFERENCES

- Ahmed, N. A., 2001.** Geomorphological and sedimentological studies on Pliocene-Quaternary alluvial fans, South Marsa Alam, Red Sea Egypt Ph.D thesis, faculty of science (Qena), South Valley University.
- Akawy, A. A., 1999.** Structural analysis of the basement complex in Wadi El Gemal area, South Eastern Desert, Egypt. Ph.D. thesis, faculty of science (Qena), South Valley University.
- Aumento, F., Laubat, H. 1971.** The Mid-Atlantic ridge near 45 N. Serpentinized ultramafic intrusions. *Can. J. Earth Sci.* Vol. XVI, 8, P. 531-863.
- Bhatia, M.R., 1983.** Plate tectonics and geochemical composition of sandstones. *J.Geol.* 91, pp 611-627.
- Elderfield, H., Hawkesworth, C.J., Greaves, M.J., Calvert, S.E., 1981.** Rare earth element geochemistry of oceanic ferromanganese nodules and associated sediments. *Geochimical Cosmochimica Acta* 45, 513-528.
- El-Desoky, H.M., 2010.** Geochemical, mineralogical and beneficiation studies on some schists bearing sillimanite refractory material, South Eastern Desert, Egypt. Philosophy Doctor Degree of Science (Geochemistry).Geology Department, Faculty of Science, Al-Azhar University.
- Fyfe, W.S., Turner, F.J., Verhoogen, J., 1958.** Metamorphic reactions and metamorphic facies. *Geol. Soc. Am. Memoir* 73.
- Hamilton, J.M., Bishop, D.T., Morris, H.C., Owens, O.E., 1982.** Geology of the Sullivan orebody, Kimberley, B.C., Canada. In: Hutchinson, R.W., Spence, C.D., Franklin, J.M. (eds.) Precambrian sulphide deposit. Geological Association of Canada. Special Paper 25, GAS, Ontario, pp. 597-665.

HanFa, Hutchinson, R.W., 1989. Evidence for exhalative origin for rocks and ores of the Dachang tin-polymetallic field. The ore-bearing formation and hydrothermal exhalative sedimentary rocks. *Mineral Deposits* 8:25-40.

Harraz, H.Z. and El Sharkawy, M. F., (2001): Origin of tourmaline in the metamorphosed Sikait politic belt, south Eastern Desert, Egypt . *Jour. Of African Earth Sciences.* v, 33, No. 2, p. 391-416.

Hegazy, H. M., 1984. Geology of wadi El-Gemal area, Eastern Desert, Egypt: Ph.D. Thesis, Assuit University., Egypt, 271 p.

Henry D.J., Guidotti C.V., 1985. Tourmaline as a petrogenetic indicator mineral: an example from the staurolite grade metapelites of NW-Maine. *American Mineralogist* 70, 1-15.

Irvine, T.N., Baragar, W.R.A., 1971. A guide to the chemical classification of the common volcanic rocks. *Can. Jour. Earth. Sc.* 8, 523-548p.

Jingwen, M., 1995. Tourmalinite from northern Guangxi, China. *Mineral Deposita*, 30, 235-245.

Khaleal, F, M., 2005. Geologic evaluation of some rare metal resources in Nugrus-sikait area, Eastern desert, Egypt. Ph.D. thesis, Al Azhar Univ. Egypt, 187p.

King, R.W., Kerrich, R.W., Daddar, R., 1988. REE distributions in tourmaline: an INAA technique involving pretreatment by B volatilization. *American Mineralogist* 73, 424-431.

Kretz, R., 1983. Symbols for rock-forming minerals. *Am. Mineral.* V. 68, 277-279p.

Lottermoser, B.G., 1989. Rare earth element study of exhalites within the Willyama Supergroup, Broken Hill block, Australia. *Mineralium Deposita* 24, 92-99.

Mahmoud, M, A M., 2005. Geological studies of episyenite and related rocks as indications to uranium concentrations in Wadi Ghadir-Wadi El Gemal area, South Eastern Desert. M.Sc. thesis, Suez Canal Univ. Egypt, 145p.

Mason, R., 1978. Petrology of the metamorphic rocks. George Allen and Unwin LTD London. 254p.

McLennan, S.M., 1989. Rare earth elements in sedimentary rocks: influence of provenance and sedimentary processes. In: Lipin, B.R., McKay, G.A. (Eds.), *Geochemistry and Mineralogy of Rare Earth Elements. Reviews Mineralogy* 21, Mineralogical Society America, Washington DC, USA, northeastern Todd County, central Minnesota. Minnesota geological survey, 1-25.

Mohamed F., H., Hassanen M., A., 1997. Geochemistry and petrogenesis of Sikait leucogranite, Egypt: an example of S-type granite in a metapelitic sequence. *Geol. Rundsch.* 86 (1997), 81-92.

Nockolds, S.R., 1947. The relation between chemical composition and paragenesis in the biotites of micas of igneous rocks. *Amer.J.Sci.* V. 245, No. 5, p. 401-420.

Pearce, J.A., Gorman, B.E., Birkett, T.G., 1975. The TiO_2 - K_2O - P_2O_5 diagram. A method of discriminating between oceanic and continental basalts. *Earth Planet. Sci. Lett.* 24, 419-426p.

Pearce, J.A., Gale, G.H., 1977. Identification of ore-deposition environment from trace element geochemistry of associated igneous host rocks. In: *Volcanic Processes in ore Genesis.* Inst. Min. and Metallurgy, Geol. Soc. London, Spec. Publ. 7, 14-24.

Pesquera, A., Velasco, F., 1997. Mineralogy, geochemistry and geological significance of tourmaline-rich rocks from the Paleozoic Cinco Villas massif (western Pyrenees, Spain). *Contributions Mineralogy Petrology* 129, 53-74.

Pettijohn, F.I., Potter, P.E., Siever, R., 1972. Sand and sandstone: Springer-Verlag, 618 p.

Roser B.P., Korsch R.G., 1986. Determination of tectonic setting of sandstone-mudstone suites using SiO₂ content and K₂O/Na₂O ratio. *Geol.*, 94, 635-650.

Saleh, G.M., 2014. Geology of Wadi El Gemal-Wadi Nugrus area, South Eastern Desert, Egypt.

Shand, S.J., 1951. "The Eruptive Rocks" John Wiley, New York.

Slack, J.F., 1996. Tourmaline associations with hydrothermal ore deposits. In: Grew E.S., Anovitz, A.M. (Eds.), *Boron; Mineralogy, Petrology and Geochemistry. Reviews in Mineralogy* 33, Mineralogical Society America, Washington DC, USA, pp. 559-643.

Slack, J.F., Palmer, M.R., Stevens, B.P.J., Barnes, R.G., 1993. Origin and significance of tourmaline-rich rock in the Broken Hill district, Australia. *Economic Geology* 88, 505-541.

Tarney, J., 1976. Geochemistry of Archaean high grade gneisses, with implications as to the origin and evolution of the Precambrian crust. In: *The Early History of the Earth*, B.F. Windly (Ed.), John Wiley, London, 405-417p.

Thompson, J.B., 1982. Composition space an algebraic and geometric approach. In J. M. Ferry, Ed., *Characterization of Metamorphism through Mineral Equilibria. Reviews in Mineralogy*, 10, 1-31.

Von Damm K.L., J.M. Edmond, B. Grant, C.I. Measures, B. Walden., R.F. Weiss. 1985. Chemistry of submarine hydrothermal solutions at 21°N, East Pacific Rise. *Geochimica et Cosmochimica Acta* 49:2, 197-220.

Yücel-Öztürk, Y., Helvacı, C., Palmer, M.R., Ersoy, E.Y., Freslon, N., 2015. Origin and significance of tourmalinites and tourmaline-bearing rocks of Menderes Massif, western Anatolia, Turkey. *Lithos* 218-219, 22-36.

Zakrutkin, V. 1968. The evolution of amphibolites during metamorphism. *Vsesoyuznaya (USSR), Mineralogicheskoe obschestvo, Zapiski (Verhandlungen)*, Vol. 97: p. 13-23.